# Lattice dynamics of superconducting zirconium and hafnium nitride halides

A. Cros,[1,*] A. Cantarero,[1] D. Beltrán-Porter,[1] J. Oró-Solé,[2] and A. Fuertes[2]
[1]*Materials Science Institute, University of Valencia, P.O. Box 22085, 46071 Valencia, Spain*
[2]*Institut de Ciència de Materials de Barcelona (CSIC), Campus UAB, 08193 Bellaterra, Spain*
(Received 3 June 2002; revised manuscript received 17 September 2002; published 3 March 2003)

We have performed a study of the Raman active modes of $\beta$-HfNCl, $\beta$-ZrNCl, and $\beta$-ZrNBr and Na-doped $\beta$-HfNCl in various scattering configurations. The experimental values are compared with a lattice dynamical calculation and assigned to definite atomic motions. The variation of the atomic force constants are analyzed as a function of the bond length, relating their relative strength with the atomic characteristics of the compound.

DOI: 10.1103/PhysRevB.67.104502 PACS number(s): 74.70.−b; 74.25.Gz; 74.25.Kc

## I. INTRODUCTION

The discovery of the superconducting layered intercalated compounds $M_x$ZrNCl, $M_x$ZrNBr and $M_x$HfNCl ($M$ = Li,Na, and $x \geqslant 0.17$), continues to attract much interest, due to their high critical temperatures for inorganic nonoxide materials and due to the possibility of controlling the critical temperature by changing their doping level.[1–3]

The compounds $\beta-MNX$ ($M$=Hf,Zr; $X$=Cl,Br) crystallize in the rhombohedral structure of SmSI type.[4–7] A view of this structure is shown in Fig. 1. An individual layer consists of double sheets $-X(MNNM)X-$. Each metal atom is bonded to three halides (on the outside of the layer), three nitrogens (on the inside of the layer), and an additional nitrogen (from the second N sheet), which describe a capped trigonal antiprism. This structure can be considered as resulting from the intercalation of N atoms in all the tetrahedral interstices inside the double metal layers of the zirconium monochloride structure, preserving the space group $R\bar{3}m$ with similar crystal parameters.[7,8] Intercalation of alcaline metals in the van der Waals gap between the double layers induces a structural transition to the polymorph YOF,[5,6] showing the same space group $R\bar{3}m$ but with a larger $c$ axis.

As has been recently stated, zirconium and hafnium nitride halides constitute an interesting system to study the physical origin of two-dimensional (2D) superconductivity. Since doping by intercalation may alter the lattice parameters of the host crystals,[9,10] it is possible to change in a controlled manner both the electrical and vibrational properties of this materials, as the separation between superconducting planes can be changed and the amount of doping may be controlled by the introduction of dopants of different size and chemical nature. In this sense, Ohashi *et al.*[11] have been able to extend the interplane distance from 9 Å for HfNCl to 18.7 Å for $Li_{0.48}$(tetrahydrofuran)$_{0.3}$HfNCl.

The electronic properties of these materials have also attracted much attention in search of an explanation for the origin of the relatively high $T_c$ temperature (around 25 K) found when the materials are conveniently doped.[4,9–13] Investigations on the vibrational properties of these compounds have been performed before.[12,14] Adelmann *et al.*[14] studied the lattice dynamics of ZrNCl and Li-intercalated ZrNCl for different polarization configurations. They showed the behavior of the Raman modes as a function of temperature and interpreted their results on the light of a lattice dynamical calculation. Weht *et al.*[12] performed an *ab initio* calculation of the fully symmetric ($A_{1g}$) Raman active vibrational modes of ZrNCl and HfNCl at the zone center, commenting on the possible role of these modes on the superconducting

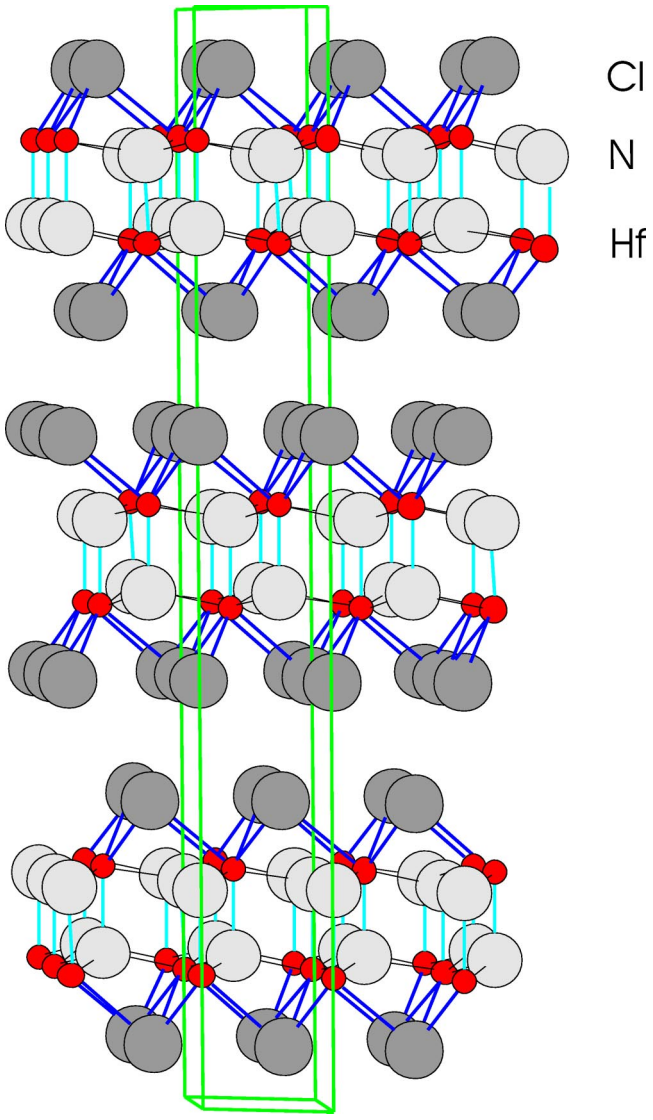


FIG. 1. Hexagonal cell showing a perspective view of the structure of $\beta$-HfNCl (Ref. 4).

 

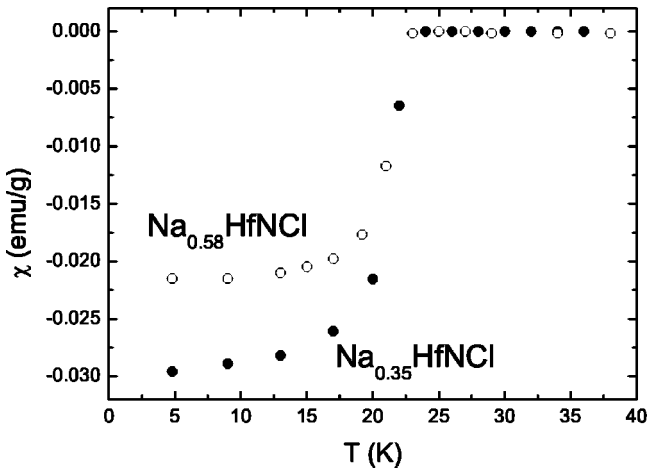


FIG. 2. Magnetic susceptibility measurements as a function of temperature showing the superconducting transition of the $Na_xHfNCl$ samples for $x=0.35$ (dots) and 0.58 (hollow dots).

behavior of the related intercalated compounds. In this work we have performed a complete study of the Raman active vibrations of superconducting $Na_xHfNCl$ and the three related nonsuperconducting halides $\beta$-HfNCl, $\beta$-ZrNCl, and $\beta$-ZrNBr. The experimental results are compared with calculations based on a force constant model. The paper is organized as follows. In Sec. II we give a brief description of sample preparation and morphology. Section III presents the experimental results of the Raman and micro-Raman measurements and in Sec. IV the experimental results are analyzed by means of the force constant model. Finally, Sec. V summarizes the conclusions of the work.

## II. SAMPLE PREPARATION

$\beta$-HfNCl, $\beta$-ZrNCl, and $\beta$-ZrNBr were prepared by the reaction of Hf (Aldrich 99.5%) or Zr (Alfa 99.9%) with $NH_4Cl$ (Aldrich 99.9%) or $NH_4Br$ (Aldrich 99.999%) at 850 °C, followed by recrystallization via vapor transport under the conditions previously reported.[4,15,16] Sodium-intercalated samples of HfNCl were prepared by dispersing the host compound $\beta$-HfNCl in a solution 1*M* of Na naphtalene in tetrahydrofuran (THF). The intercalation reactions were done in an Ar-filled glove box at room temperature for a period of 20 h. The samples were characterized by chemical analysis, powder x-ray diffraction, and magnetic susceptibility measurements. The magnetic susceptibility measurements have been performed in a Quantum Design superconducting quantum interference device (SQUID) magnetometer down to 4 K. The samples were double sealed in Ar atmosphere. These measurements are shown in Fig. 2, from which a superconducting transition around 23 K can be deduced for both samples.

X-ray diffraction patterns for the sodiated samples were taken on an INEL curved position-sensitive CPS120 powder diffractometer by using 0.1 mm capillaries sealed under Ar as sample holders. The angular range was 120° and the radiation was Cu $K\alpha_1$, obtained with a Ge(111) monochromator.[4]

The material obtained has the form of small particles with hexagonal platelet morphologies and a broad distribution of particle sizes ranging from 2 to 200 $\mu$m. The particles have a strong preferential orientation along the hexagonal *c* axis. Samples doped with Na were sealed in glass capillaries (wall thickness $\approx$0.01 mm, diameter $\approx$0.1 mm) filled with argon gas to avoid the reaction of samples with the atmosphere.

## III. RAMAN MEASUREMENTS

The Raman spectra were obtained at room temperature with a Dilor XY-800 triple spectrometer in the subtractive dispersion mode (resolution $\approx 1$ cm$^{-1}$), equipped with a nitrogen-cooled charged coupled device (CCD) multichannel detector. The laser beam was focused either by a photographic objective with 85 mm of focal length or a 50× microscope objective. Different $Ar^+$ laser lines (514.5, 488, and 476 nm) were used for excitation to investigate resonance effects. The laser power was kept around 50 mW. To obtain Raman spectra with a known scattering configuration, we selected from the samples the biggest particles, typically sized $200\times200\times20$ $\mu$m$^3$. After studying the morphology of the particles under an optical microscope, we selected for measurement those with a more obvious plateletlike morphology. The spectra of particles exhibiting disorder along the *c* axis was also recorded for comparison. Raman spectra of the selected particles were recorded in the backscattering configuration for both parallel and crossed polarizations of the incoming and scattered light and with the light incident along the *c* axis and perpendicular to it. The scattering configuration is indicated in each spectra by means of the Porto notation. In all samples, the *z* direction has been taken along the *c* axis.

The process of particle selection was not possible for the Na-doped samples kept in the quartz capillary, where the direction of incidence of the light with respect to the *c* axis was arbitrary, although the platelet habit of the particles fa-

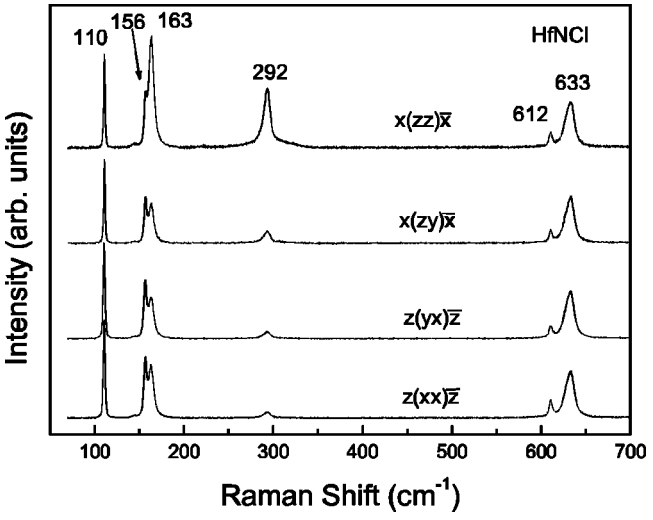


FIG. 3. Room temperature Raman spectra of the $\beta$-HfNCl sample for different polarization configurations. The *z* direction is taken along the *c* axis. The 514.5 nm line of an Ar-ion laser has been used for excitation.

TABLE I. Energies $\omega$ ($cm^{-1}$), linewidths (full width at half maximum) $\Gamma$ ($cm^{-1}$), symmetries, and assignments of the observed (expt) and calculated (theor) phonon modes. The atoms involved in the vibration are shown in Fig. 6.

| | | $E_g$ | $E_u$ | $A_{2u}$ | $A_{1g}$ | $A_{1g}$ | $A_{1g}$ | $E_g$ | $A_{2u}$ | $E_g$ | $E_u$ | $A_{2u}$ [a] | $E_u$ [a] |
|---|---|---|---|---|---|---|---|---|---|---|---|---|---|
| HfNCl | $\omega_{expt}$ | 633 | | | 612 | 292 | 163 | 156 | | 110 | | | |
| | $\omega_{theor}$ | 634 | 632 | 617 | 613,604 [b] | 290,386 [b] | 163,191 [b] | 157 | 128 | 105 | 105 | | |
| | $\Gamma$ | 11 | | | 4 | 10 | 7 | 4 | | 2 | | | |
| $Na_{0.58}HfNCl$ | $\omega_{expt}$ | 620 | | | 593 | 281 | 149 | 158 | | 107 | | | |
| | $\omega_{theor}$ [c] | 620 | 618 | 596 | 594 | 279 | 146 | 162 | 183 | 111 | 146 | 108 | 85 |
| | $\Gamma$ | 23 | | | $>50$ | 13 | 10 | 8 | | 4 | | | |
| $Na_{0.35}HfNCl$ | $\omega_{expt}$ | 616 | | | 595 | 282 | 147 | 157 | | 106 | | | |
| | $\Gamma$ | 32 | | | $>40$ | 12 | 13 | 8 | | 4 | | | |
| ZrNBr | $\omega_{expt}$ | 583 | | | | 297 | 141 | 171 | | 87 | | | |
| | $\omega_{theor}$ | 584 | 580 | 583 | 583 | 297 | 147 | 168 | 140 | 86 | 106 | | |
| | $\Gamma$ | 9 | | | | 20 | 4 | 3 | | 3 | | | |
| ZrNCl | $\omega_{expt}$ | 605,604 [d] | | | 591,590 [d] | 331,326 [d] | 191,187 [d] | 184,179 [d] | 165 [d] | 128,123 [d] | | | |
| | $\omega_{theor}$ | 605 | 605 | 592 | 591,586 [b] | 331,334 [b] | 192,202 [b] | 184 | 154 | 119 | 126 | | |
| | $\Gamma$ | 9 | | | 7 | 20 | 3 | 4 | | 3 | | | |
| $Li_{0.16}ZrNCl$ [d] | $\omega_{expt}$ | 608 | | | 582 | 322 | 188 | 178 | | 123 | | | |

[a]These two modes appear after the intercalation of Na atoms in the structure.
[b]*Ab initio* calculations performed in Ref. 12.
[c]These calculations have been performed for $Na_{0.5}HfNCl$.
[d]Values taken from Ref. 14.

vors the incidence along the direction of the $c$ axis. In all spectra shown, plasma lines have been used to check the spectrometer calibration, but have been subtracted in the presentation for clarity.

From group theory considerations[17] we expect six Raman active modes for the $\beta-MNX$ structure belonging to the space group $R\bar{3}m$, with the six atoms of the unit cell occupying $6c$ Wyckoff positions. Three of these modes belong to the $A_{1g}$ symmetry. The other three vibrational modes belong to the doubly degenerate $E_g$ symmetry. Besides these six Raman active modes, group theory predicts four ir active $(2A_{2u}+2E_u)$ symmetry modes. Since the space group $R\bar{3}m$ is centrosymmetric, Raman and ir active modes are mutually excluded. The last three vibrations $(A_{2u}+E_u)$ correspond to the translational (acoustic) modes of the crystal.

When introducing the Na doping, the crystal retains its symmetry, with the Na atoms going into $3a$ Wyckoff sites (position (000)) and the metal and nitrogen atoms interchanging their positions.[2] The new atoms, occupying a site of $\bar{3}m$ symmetry, introduce two ir active modes of symmetries $A_{2u}+E_u$ but no new Raman active modes.

Figure 3 shows the Raman spectra obtained for $\beta$-HfNCl in four different polarization configurations, with the incident and scattered light propagating along the $c$ axes [indicated as $z(xx)\bar{z}$ and $z(yx)\bar{z}$] or perpendicular to it [$x(zz)\bar{x}$ and $x(zy)\bar{x}$]. As symmetry arguments indicate, six Raman active phonon modes can be distinguished in the spectra, at energies of 110, 156, 163, 292, 612, and 633 $cm^{-1}$. The two peaks appearing at higher energy (633 and 612 $cm^{-1}$) are easily assigned to the oscillations of nitrogen, the lightest atom in the molecule. The origin of the other vibrations will be discussed later. The Raman spectra of the samples have been measured for different lines of the $Ar^+$-ion laser, but no resonant enhancements of the signals have been found so far.

Concerning the symmetry of the modes, the only nonzero elements of the polarizability tensor with symmetry $A_{1g}$ are the diagonal elements $\alpha_{xx}+\alpha_{yy},\alpha_{zz}$, while those with symmetry $E_g$ are $\alpha_{xx}-\alpha_{yy},\alpha_{xy}$ and $\alpha_{xz},\alpha_{yz}$, reflecting the anisotropy of the crystal along the $c$ axis and perpendicular to it. In backscattering from the $c$ axis ($z$ direction), the $A_{1g}$ modes would be Raman active only in parallel polarization, while the modes with $E_g$ symmetry would be allowed both

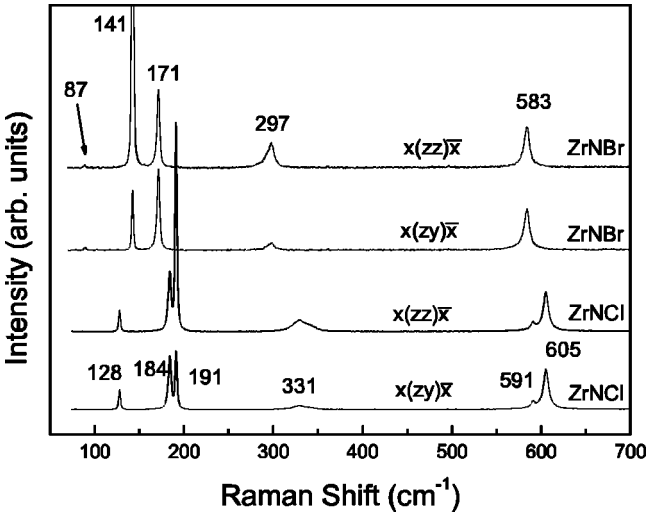


FIG. 4. Room temperature Raman spectra of the $\beta$-ZrNCl sample (lower two spectra) and $\beta$-ZrNBr (upper two spectra) for different polarization configurations. The $z$ direction is taken along the $c$ axis. The 514.5 nm line of an Ar-ion laser has been used for excitation.

TABLE II. Parameters used in the force constants for the different samples. The values of the force constants are given in units of $10^5$ dyn/cm. $M$ represents the metal atom (Hf or Zr) and $X$ the halogen atom (Cl or Br).

| | $M$-N short bond | $M$-N long bond | $M-X$ | $M-M$ | $X-X$ |
|---|---|---|---|---|---|
| HfNCl | 2.09 | 2.61 | 0.23 | 2.16 | 0.07 |
| ZrNCl | 1.76 | 2.26 | 0.29 | 1.48 | 0.11 |
| ZrNBr | 1.59 | 2.25 | 0.38 | 1.16 | 0.13 |
| $Na_{0.5}$HfNCl | 1.98 | 2.49 | 0.24 | 2.14 | 0.10 [a] |

[a]Force constant along the Cl-Na bond.

for parallel and crossed polarizations. This selection rule fails clearly in the experimental spectra (first two spectra at the bottom of Fig. 3), as none of the modes disappears. This means that, although we have selected sample particles with a plateletlike morphology, there is still enough misalignment to render the mode symmetry assignment very difficult for backscattering from the $c$ axis.

To accomplish the mode assignment, we have repeated the experiments in backscattering configuration from a direction perpendicular to the $c$ axis ($x$ direction). As shown in the top two spectra of Fig. 3, there is an evident increase in intensity of the lines at 163 and 292 $cm^{-1}$ when going from crossed ($zy$) to parallel ($zz$) polarization, and a slight increase of the mode at 612 $cm^{-1}$. Consequently, we assign these three modes to $A_{1g}$ symmetry, while the other three (appearing at 110, 156, and 633 $cm^{-1}$) are ascribed to vibrations in the $xy$ plane ($E_g$ symmetry). The increase of the intensity of the $A_{1g}$ modes for ($zz$) polarization with respect to the ($xx$) polarization is due to the high anisotropy of the crystal: the value of the polarizability along $c$, $\alpha_{zz}$, is considerably larger than that of $\alpha_{xx}=\alpha_{yy}$, as shown in the experiment. The value of the $A_{1g}$ modes measured for HfNCl (163, 292, 612 $cm^{-1}$) are to be compared with the corresponding *ab initio* calculations performed by Weht *et al.*,[12] of 191, 386, and 604 $cm^{-1}$ (see Table I). A similar polarization study has been performed for $\beta$-ZrNCl and $\beta$-ZrNBr (Fig. 4), and the symmetry of the Raman active modes has been assigned according to their polarization behavior, following the arguments considered for $\beta$-HfNCl above. As in the analysis performed for $\beta$-HfNCl, the spectra present very slight changes when comparing $z(xx)\bar{z}$ and $z(xy)\bar{z}$ configurations (not shown), while the intensity differences are larger between $x(zz)\bar{x}$ and $x(zy)\bar{x}$ configurations. The final assignments are given in Table I. The values measured for the $A_{1g}$ modes of ZrNCl (191, 331, and 591 $cm^{-1}$) may again be compared to the values calculated by Weht *et al.*[12] of 202, 334, and 586 $cm^{-1}$ and agree with those measured by Adelmann *et al.*[14] to within 10%.

The spectra obtained for $\beta$-ZrNBr (upper two spectra of Fig. 4) deserve additional comments. As for the other two compounds with the same crystal structure, group theory predicts six Raman active modes. However, in the spectra we find only four clear modes at 141, 171, 297, and 583 $cm^{-1}$, and a very weak mode at 87.5 $cm^{-1}$. There is one mode missing, which we believe is accidentally degenerate with the mode appearing at 583 $cm^{-1}$. We will return to this point later on.

Figure 5 shows the Raman spectra obtained for two Na-intercalated HfNCl samples with compositions $Na_{0.35}$HfNCl and $Na_{0.58}$HfNCl. Both samples showed a superconducting transition with $T_c \approx 23$ K, as previously shown in Fig. 2. The Raman spectrum of undoped $\beta$-HfNCl has been included for reference. No changes have been observed between parallel and perpendicular polarizations. As a consequence of doping, the lines shift to lower energies and broaden presumably due to the disorder introduced in the lattice. The shift is more pronounced for the high-energy modes. Moreover, although the changes introduced by the intercalation are similar for both concentrations of Na, the high-energy mode shifts to higher frequency with the amount of Na from 616 $cm^{-1}$ for $x=0.35$ to 620 $cm^{-1}$ for $x=0.58$. All the modes broaden between 50% and 100%. However, the broadening of one of the modes, the $A_{1g}$ at 612 $cm^{-1}$, increases enormously after intercalation.

Although the inclusion of Na atoms does not generate new Raman active modes, the changes in crystal structure are considerable:[2] there is a variation in $c$ close to 7%, and the metal and nitrogen atoms interchange their positions. The wavelengths and linewidths of the different phonon modes are summarized in Table I.

To acquire a better understanding of the atomic motions involved in the vibrational modes and the changes that originate from the difference in crystal parameters and atomic masses among $\beta$-HfNCl, $\beta$-ZrNCl, and $\beta$-ZrNBr, we have performed a lattice dynamical calculation using a force constants. For the intercalated samples, the calculations have been performed for $x=0.5$, corresponding to full occupancy of the octahedral sites in the van der Waals gap by the Na atoms. The results are discussed in the following section.

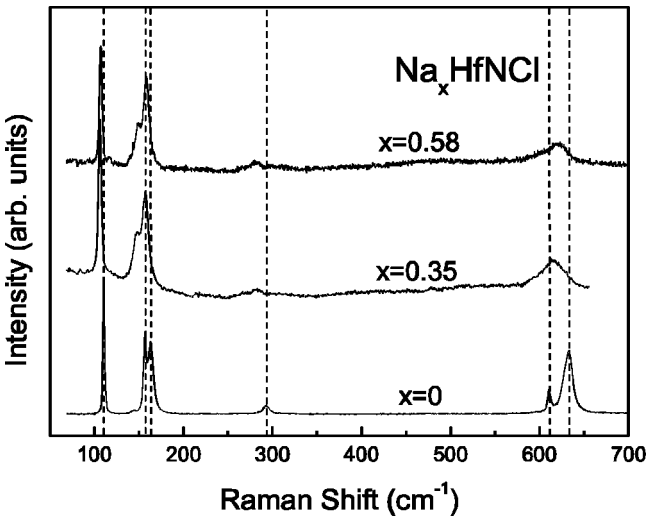


FIG. 5. Room temperature Raman spectra of the $\beta-Na_xHfNCl$ samples for $x=0.35$ and $x=0.58$. The spectrum for an undoped HfNCl sample in the $z(xx)\bar{z}$ polarization configuration has been included for comparison.

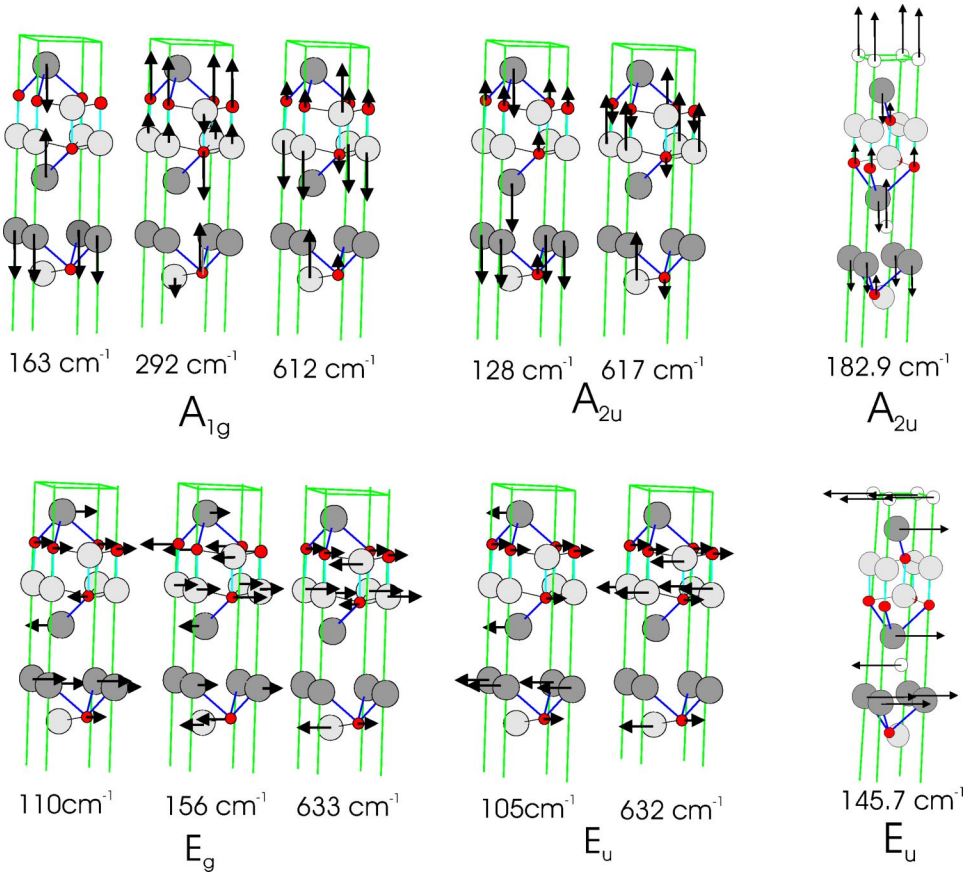


FIG. 6. Hexagonal cell showing the atomic displacements corresponding to the different vibrational modes. Since the space group $R\bar{3}m$ is centrosymmetric, only half of the hexagonal cell is shown here. The wave numbers correspond to HfNCl. The small balls represent metal atoms, the dark big balls halogen atoms and the gray ones represent nitrogens. In the modes labeled $A_{2u}$ and $E_u$ at the right-hand side of the figure, the hexagonal cell reflects the modifications due to the intercalation of Na atoms in $Na_{0.5}HfNCl$. These figures show the movement of the atoms for the two new modes originated after intercalation.

## IV. LATTICE DYNAMICS

In the force constant model, the atoms are assumed to be point charges interacting by a model potential. The short-range interaction potential is chosen to depend exponentially on the relative distance between the ions (Born-Mayer potential), and the force constants (bond stretching and bond bending) are derivatives of this potential, taken at the equilibrium position. For a full description of the model, interested readers are directed to the appropriate literature;[1] see, for example, Refs. 18 and 19. Five parameters have been used in the model in order to calculate the 18 atomic vibrations of each crystal, six of which are Raman active. The values of these parameters are shown in Table II for the four samples studied.

The two first parameters correspond, in increasing order of bond length, to the two types of metal-nitrogen bonding present in the crystal. The first relates to the bond perpendicular to $c$ and the second to that parallel to $c$. The third parameter corresponds to bonds between neighboring metal halogen atoms. The remaining two parameters relate to second-neighbor interactions among the metal atoms and the halogen atoms. In the case of $Na_{0.5}HfNCl$, the last parameter corresponds to the Cl-Na bonding. The value of the bond parameters decreases exponentially as a function of bond length, as expected from the force constants. The relative importance of the force constants between neighboring metal atoms stands out. This importance can be understood by noticing that the high value also accounts for the bending strength of the metal-nitrogen bond, as indicated before. Moreover, as reported in Ref. 3 although the extended metal-metal bonding of ZrCl is not present in $\beta$-ZrNCl, there is still an overlap population of 0.019 for Zr-Zr bonding (3.35 Å) that has its origin in two $t_{2g}$ orbitals that are left for metal-metal interactions after the formation of the metal-nitrogen bondings, increasing the bond strength further. In Table I the energy modes obtained with this model are compared with those of the experiment. We have included as well the values of the calculated ir active modes for completeness. Observe that, although the agreement is in general very good, the discrepancy increases for the two lower-energy modes with $E_g$ symmetry. The reason for this disagreement is the strong coupling between these modes, which are very close in energy and belong to the same symmetry. Notice that for $\beta$-ZrNBr the highest-energy modes, associated with nitrogen vibrations along and perpendicular to $c$, are degenerate. This degeneracy is accidental and is allowed by symmetry arguments, as the two vibrations involved belong to two different representations.

The analysis of the mode vibrations by means of the force constant model allows us to visualize the normal coordinates that describe the movement of the atoms for the different modes, as shown in Fig. 6 for $\beta$-HfNCl. The displacement of the atoms are similar for $\beta$-ZrNCl and $\beta$-ZrNBr, although small differences may be present due to the different masses of the atoms involved in the vibrations. In the figure, the arrows indicate the direction of the movement and their length gives an approximate measure of the relative amplitude of the oscillations. Since the space group $R\bar{3}m$ is centrosymmetric, we have represented only half of the hexagonal cell of the crystal. The direction of the atomic displacements in the omitted lower part of the cell is the same as that shown for the *ungerade* modes and opposite for the *gerade* modes.

As expected from group theory, modes with $A_{1g}$ and $A_{2u}$ symmetry correspond to atomic oscillations along the *c* axis, while those belonging to the doubly degenerate $E_g$ and $E_u$ representations oscillate in the plane perpendicular to *c*. The equivalent vibrations are obtained rotating the figures 90° around the *c* axis. We will concentrate in the analysis of the normal modes of the Raman active vibrations, which are the ones measured in this work.

The mode of lowest energy belongs to the $E_g$ representation. These mode involves the movement of the halogen and metal atoms in phase, the contribution of the N atoms being negligible for HfNCl. When substituting Hf for Zr, considerably lighter (compare 178.5 with 91.22 amu), the contribution of the nitrogen atoms to the vibration increases, vibrating out of phase with the metal and halogen atoms. The amplitude of vibration of nitrogen in this mode is approximately half of that of the metal atom for ZrNCl and ZrNBr. This is a bending mode in which the upper half of each layer slides away-from the bottom part. Increasing the energy, we find two modes that vibrate with similar frequency. One belongs to the $A_{1g}$ representation. The movement of the halogen atoms contributes mostly to this mode, vibrating out of phase in each layer (stretching mode). The substitution of Cl by Br in ZrN*X* lowers the energy of this $A_{1g}$ mode considerably, due to the increase of mass of the substituted atom (35.45 vs 79.90 amu). The normal coordinates describing the $E_g$ mode that appears at a similar energy is more complicated, showing contributions of all the atoms of the layer. The nitrogen and metal atoms vibrate in phase, while the halogen atoms vibrate out of phase, producing a combination of stretching and bending. As discussed before, the substitution of Hf by Zr results in the increase of the relative amplitude of the nitrogen atom in the vibration.

Below the highest-energy modes there is an energy gap where we only find one vibrational mode with $A_{1g}$ symmetry. This mode arises essentially from the movement of the metal atoms, although nitrogen atoms oscillate with smaller amplitude out of phase with the metal (stretching mode). In Ref. 12 this mode is attributed to the $M-X$ ($X$ is the halogen atom) vibration moving out of phase.

Finally, we find the modes that arise from the movement of the lightest atoms, and thus involve mainly nitrogen, although there is a small contribution of the metal atoms moving out of phase with respect to the nitrogen atoms of the same layer. The $E_g$ mode is similar, but the movement of the atoms is perpendicular to the *c* axis. In the compounds studied, the doubly degenerate $E_g$ mode appears at higher energy than the corresponding $A_g$, but for ZrNBr these modes are accidentally degenerated.

After intercalation, the Na atoms occupy the positions at the corners of the cell and equivalent positions in the van der Waals gap between two adjacent layers.[2] The new structure is shown in the two hexagonal cells on the right-hand side of Fig. 6 and has been represented for $Na_{0.5}$HfNCl. As the Na atoms occupy a site with inversion symmetry, the intercalated atoms do not contribute to Raman scattering. With respect to the ir active *ungerade* modes, as indicated in Sec. III, the new atoms introduce two new vibrations, of symmetries $A_{2u}$ and $E_u$, which appear at 85 and 108 $cm^{-1}$, respectively, in our calculations. The movement of the atoms for these modes is shown in the two cells at the right-hand side of Fig. 6, where the Na atoms (white) move in counterphase with the halogen atoms. In the rest of the *ungerade* modes the Na atoms move in phase with the halogen atoms. As we have commented before, the effect of the intercalation is to shift the modes to lower energy and increase their broadening. The mode with the most drastic change in the broadening (more than 40–50 $cm^{-1}$ of the linewidth—full width at half maximum) is related to N-Hf vibrations (see Fig. 6, $A_{1g}$ mode at 612 $cm^{-1}$). Within a layer, the upper half-layer vibrates in opposite phase to the lower half-layer. This mode could be related to the superconducting properties of these materials, as has been suggested in Ref. 14, since the bands near the Fermi edge have mainly metal-nitrogen character.[12]

## V. CONCLUSIONS

We have characterized the vibrations of $\beta$-HfNCl, $\beta$-ZrNCl, $\beta$-ZrNBr, and $Na_x$HfNCl, with $x=0.35$ and 0.58. From the measurements of the modes for different scattering configurations, we have assigned the symmetry of the vibrations, discussing the normal coordinates that describe the atomic motions for each mode. Comparison with the force constant model allows us to determine the relative importance of the metal-metal bonding in these compounds. One of the Raman modes ($A_{1g}$ mode at 612 $cm^{-1}$ for HfNCl) experiences a huge broadening after the intercalation of Na atoms. This mode may be related to superconductivity, as it involves the movement of nitrogen and hafnium atoms, and the metal-nitrogen layers carry the superconducting current.

## ACKNOWLEDGMENT

We would like to thank the Ministry of Science and Technology (Grant No. PB1998-1424-CO2), The Comissionat por Universitats i Recerca de la Generalitat de Catalunya (CIRIT, Grant No. 2000SGR 00113), and the European Union for financial support. Dr. B. Martínez is acknowledged for SQUID measurements. The authors wish to thank Z. Popović for helpful suggestions.

*Electronic address: Ana.Cros@uv.es

[1] S. Yamanaka, H. Kawaji, K. Hotehama, and H. Kawaji, Nature (London) **392**, 580 (1998).
[2] S. Shamoto, K. Iizawa, M. Yamada, K. Ohoyama, Y. Yamaguchi, and T. Kajitani, J. Phys. Chem. Solids **60**, 1431 (1999).
[3] M. Vlassov, M.R. Palacín, D. Beltrán-Porter, J. Oró-Solé, E. Canadell, P. Alemany, and A. Fuertes, Inorg. Chem. **38**, 4530 (1999).
[4] A. Fuertes, M. Vlassov, D. Beltrán-Porter, P. Alemany, E. Canadell, N. Casañ-Pastor, and M.R. Palacín, Chem. Mater. **11**, 203 (1999).
[5] S. Shamoto, T. Kato, Y. Ono, Y. Miyazaki, K. Ohoyama, M. Ohashi, Y. Yamaguchi, and T. Kajitani, Physica C **306**, 7 (1998).
[6] F. Hulliger, *Structural Chemistry of Layer Type Phases*, edited by F. Lévy (Reidel, Dordrecht, 1979), Vol. 5.
[7] J.E. Ford, J.D. Corbett, and S. Hwu, Inorg. Chem. **22**, 2789 (1983), and references therein.
[8] D.G. Adolphson, J.D. Corbet, Inorg. Chem. **15**, 1820 (1976).
[9] H. Tou, Y. Maniwa, T. Koiwasaki, and S. Yamanaka, Phys. Rev. Lett. **86**, 5775 (2001).
[10] S. Yamanaka, H. Kawaji, K. Hotehama, and M. Ohashi, Adv. Mater. **8**, 771 (1996).
[11] M. Ohashi, T. Shigeta, S. Yamanaka, and M. Hattori, J. Electrochem. Soc. **136**, 1086 (1989).
[12] R. Weht, A. Filippetti, and W.E. Pickett, Europhys. Lett. **48**, 320 (1999).
[13] I. Hase and Y. Nishihara, Phys. Rev. B **60**, 1573 (1999).
[14] P. Adelmann, B. Renker, H. Schober, M. Braden, and F. Fernández-Díaz, J. Low Temp. Phys. **117**, 449 (1999).
[15] A. Fuertes, M. Vlassov, D. Beltrán-Porter, and M. R. Palacín-Peiró, Patent No. 9901978, Oficina Española de Patentes y Marcas, Spain (1999).
[16] J. Oró-Solé, M. Vlassov, D. Beltrán-Porter, M.T. Caldés, V. Primo, and A. Fuertes, Solid State Sci. **4**, 475 (2002).
[17] D.L. Rousseau, R.P. Bauman, and S.P.S. Porto, J. Raman Spectrosc. **10**, 253 (1981).
[18] P. Brüesch, in *Phonons: Theory and Experiment I, Lattice Dynamics and Models of Interatomic Forces*, Vol. 34 of Springer Series in Solid State Sciences (Springer, Heidelberg, 1982).
[19] A. A. Maradudin, E. W. Montroll, G. H. Weiss, and I. P. Ipatova, *Theory of Lattice Dynamics in the Harmonic Approximation* (Academic Press, New York, 1971).